

UC San Diego

UC San Diego Previously Published Works

Title

Modeling hypercholesterolemia and vascular lipid accumulation in LDL receptor mutant zebrafish

Permalink

<https://escholarship.org/uc/item/8xn74812>

Journal

Journal of Lipid Research, 59(2)

ISSN

0022-2275

Authors

Liu, Chao

Kim, Young Sook

Kim, Jungsu

et al.

Publication Date

2018-02-01

DOI

10.1194/jlr.d081521

Copyright Information

This work is made available under the terms of a Creative Commons Attribution License, available at <https://creativecommons.org/licenses/by/4.0/>

Peer reviewed



Modeling hypercholesterolemia and vascular lipid accumulation in LDL receptor mutant zebrafish[§]

Chao Liu,* Young Sook Kim,*[†] Jungsu Kim,* Jennifer Pattison,* Andrés Kamaid,^{§,***} and Yury I. Miller^{1,*}

Department of Medicine, University of California, San Diego,* La Jolla, CA; Korean Medicine Convergence Research Division, Korea Institute of Oriental Medicine Republic of Korea,[†] Daejeon, South Korea; Analytical Biochemistry and Proteomics Unit[§] and INDICyO Institutional Program,^{**} Institut Pasteur de Montevideo, Montevideo, Uruguay

Abstract Elevated plasma LDL cholesterol is the dominant risk factor for the development of atherosclerosis and cardiovascular disease. Deficiency in the LDL receptor (LDLR) is a major cause of familial hypercholesterolemia in humans, and the LDLR knockout mouse is a major animal model of atherosclerosis. Here we report the generation and characterization of an *ldlr* mutant zebrafish as a new animal model to study hypercholesterolemia and vascular lipid accumulation, an early event in the development of human atherosclerosis. The *ldlr* mutant zebrafish were characterized by activated SREBP-2 pathway and developed moderate hypercholesterolemia when fed a normal diet. However, a short-term, 5-day feeding of *ldlr* mutant larvae with a high-cholesterol diet (HCD) resulted in exacerbated hypercholesterolemia and accumulation of vascular lipid deposits. Lomitapide, an inhibitor of apoB lipoprotein secretion, but not the antioxidant probucol, significantly reduced accumulation of vascular lipid deposits in HCD-fed *ldlr* mutant larvae. Furthermore, *ldlr* mutants were defective in hepatic clearance of lipopolysaccharides, resulting in reduced survival. Taken together, our data suggest that the *ldlr* knockout zebrafish is a versatile model for studying the function of the LDL receptor, hypercholesterolemia, and related vascular pathology in the context of early atherosclerosis.—Liu, C., Y.S. Kim, J. Kim, J. Pattison, A. Kamaid, and Y. I. Miller, **Modeling hypercholesterolemia and vascular lipid accumulation in LDL receptor mutant zebrafish.** *J. Lipid Res.* 2018. 59: 391–399.

Supplementary key words low density lipoprotein receptor • atherosclerosis • lipid deposit

This study was supported by National Institutes of Health Grants HL135737 and HL088093 (Y.I.M.) and American Heart Association Grant 16POST27250126 (C.L.). Y.S.K. was supported by the long-term international fellowship program from the Korea Institute of Oriental Medicine. A.K. was supported by the “Programa de Desarrollo de las Ciencias Básicas” and by the Agencia Nacional de Investigación e Innovación, Uruguay (Grant ALI_2_2014_1_5055; Carlos Escande and Carlos Batthyany, principal investigators). The content is solely the responsibility of the authors and does not necessarily represent the official views of the National Institutes of Health.

Manuscript received 30 October 2017 and in revised form 11 November 2017.

Published, *JLR Papers in Press*, November 29, 2017

DOI <https://doi.org/10.1194/jlr.D081521>

The relationship between LDL cholesterol (LDL-C) and risk of cardiovascular disease (CVD) has been well established through numerous epidemiological observational and genetics studies and interventional clinical trials (1). Liver expression of the LDL receptor (LDLR) is a major factor in regulation of plasma levels of LDL-C (2, 3). Human patients with loss-of-function *LDLR* gene variants develop familial hypercholesterolemia (FH) (1, 4–6), and homozygous FH patients develop advanced atherosclerotic lesions at an early age (4, 5, 7). Expression of LDLR as well as the expression of proteins involved in biosynthesis of cholesterol, such as HMG-CoA reductase (HMGCR), are regulated by the transcription factor SREBP-2, which in turn is regulated by intracellular cholesterol levels (8).

Therapies targeting LDLR expression, such as statins and recently, proprotein convertase subtilisin-kexin type 9 (PCSK9) antibodies, have been successful in lowering LDL-C and reducing incidence of CVD. However, LDLR targeting has its limitations, and there remains a large need for developing drugs targeting non-LDLR pathways. Examples of such non-LDLR pathway therapies include lomitapide, an inhibitor of microsomal triglyceride transfer protein (MTP), and mipomersen, an antisense oligonucleotide targeting apoB mRNA. These two drugs inhibit assembly and secretion of hepatic and intestinal lipoproteins (9). In addition, an antibody targeting angiopoietin-like 3 resulted in a significant reduction of LDL-C in homozygous FH patients (10).

Animal models in which LDLR has been incapacitated may serve to identify new, LDLR-independent targets to treat hypercholesterolemia. *Ldlr*^{-/-} mice (11, 12) have been instrumental in understanding mechanisms of atherosclerosis,

Abbreviations: dpf, days postfertilization; FH, familial hypercholesterolemia; HCD, high-cholesterol diet; HMGCR, HMG-CoA reductase; LDL-C, LDL cholesterol; LDLR, LDL receptor; LPS, lipopolysaccharide; ORO, Oil Red O; TG, triglyceride.

¹To whom correspondence should be addressed.

e-mail: yumiller@ucsd.edu

[§]The online version of this article (available at <http://www.jlr.org>) contains a supplement.

but their use for drug screening is limited because expensive, time-consuming, and labor-intensive procedures are involved in the analysis of atherosclerosis. In contrast, the use of zebrafish is cost-effective because of large progeny numbers and low maintenance costs. Transparent zebrafish larvae are suitable for live imaging, and a quick staining protocol for lipids and easy genetic manipulation allow for effective screening. Recently, new zebrafish models emerged to investigate aspects of lipoprotein metabolism, lipid abnormalities, and atherosclerosis (13–15). Importantly, genes involved in lipid and lipoprotein metabolism, including *APOB*, *APOA* family, *APOC2*, *LPL*, *CETP*, and *LDLR*, are conserved between humans and zebrafish (16–18).

Particularly, *Ldlr*, which is responsible for LDL uptake in liver, has been reported to be functionally conserved in zebrafish. Transient knockdown of *ldlr* with antisense morpholino oligonucleotides leads to higher LDL-C levels and vascular lipid deposits after feeding a high-cholesterol diet (HCD) (19). To further improve robustness and simplify the experimental procedure, we generated a genetic zebrafish model in which an *ldlr* mutation achieved by using the CRISPR/Cas9 approach resulted in hypercholesterolemia and robust vascular lipid accumulation following a very short, 5-day HCD feeding. Our data provide evidence that the *ldlr* mutant zebrafish is a versatile model to study hypercholesterolemia and related vascular pathology.

MATERIALS AND METHODS

Zebrafish maintenance and feeding

Adult zebrafish of the AB strain were maintained at 28°C on a 14 h light/10 h dark cycle and fed brine shrimp twice a day. Zebrafish larvae were fed Golden Pearls (100- to 200- μ m size from Brine Shrimp Direct) twice a day, starting from 4.5 days postfertilization (dpf). For HCD feeding, 4% weight per weight (w/w) cholesterol (Sigma, 362794) were added to Golden Pearls, as reported (14, 20). For drug treatment experiments, lomitapide (Cayman, 10009610) or probucol (Cayman, Catalog no. 15043), together with cholesterol, were dissolved in diethyl ether (Spectrum, E1010) and thoroughly mixed with Golden Pearls. After diethyl ether evaporation, content of lomitapide was 0.14% w/w, and probucol 0.05% w/w. For visualization of vascular lipid deposits, the same method was used to supplement Golden Pearls with 1 μ g/g of a fluorescent cholesteryl ester analog (cholesteryl BODIPY 576/589-C11, Invitrogen, C12681), as previously described (13). All animal studies were approved by the University of California, San Diego institutional animal care and use committee.

CRISPR/Cas9 mediated *Ldlr* knockout in zebrafish

pT3TS-zCas9 and T7-gRNA plasmids were from the Chen lab (21) through Addgene. Following the published protocol, we synthesized nls-zCas9-nls mRNA with a mMESSAGE mMACHINE T3 kit (ThermoFisher, AM1348) and recovered with lithium chloride precipitation. *ldlr* gRNA was generated using a MEGAscript T7 kit (ThermoFisher, AM1354) and purified with a mirVana miRNA isolation kit (ThermoFisher, AM1560). The zebrafish *ldlr* genomic target sequence was 5'-ggttgactgccgactgccgTGG-3' in which the first 20 nt was the gRNA template and the last 3 nt was

protospacer adjacent motif required for CRISPR/Cas9 function. We injected 30 pg *ldlr* gRNA and 150 pg nls-zCas9-nls mRNA into 1- to 2-cell stage embryos. The genomic DNA (gDNA) was extracted from whole embryos or from adult tail tissue by using a KAPA Express Extract Kit (KAPA Biosystems, KR0383). The gDNA fragment containing the target site was amplified using KOD DNA polymerase (EMD Millipore, 71086) and digested with T7 endonuclease (NEB, M0302). Primers used for PCR amplification of *ldlr* gDNA fragment were 5'-tcgttatgggacgtctgtga-3' and 5'-tatgtagaccaactaccgac-3'. Primers used for PCR amplification of *ldlr* cDNA flanking exon 2 to exon 7 were 5'-agttgtggtggtcactaaa-3' and 5'-atgtcttcacagcgtctctt-3'.

Triglyceride and total cholesterol measurements and lipoprotein analysis

Blood was collected from adult zebrafish, 4 h after feeding, through tail amputation and diluted 1:200 in PBS. Five dpf larvae were gently homogenized in PBS with pestle. After centrifugation, supernatants were collected and referred to as "homogenate." Triglyceride (TG) and total cholesterol levels in diluted plasma or larvae homogenate were measured with kits according to manufacturer's protocol (Biovision, Triglyceride Quantification Kit, K622-100; Cholesterol Quantification Kit, K623-100). Lipoprotein fractions were assessed using native agarose gel electrophoresis (Helena Laboratories, 3045) as we previously described (13).

Fast protein liquid chromatography lipoprotein profile

A total of 50 to 60 μ l of pooled plasma from 20 to 30 adult WT, *ldlr* mutant, and *apoc2* mutant zebrafish were loaded onto a Superose 6 PC 3.2/30 column (GE Healthcare Life Science, 17-0673-01), and total cholesterol and TG levels were determined in each fraction (250 μ l), collected at a flow speed of 0.5 ml/min.

Quantitative RT-PCR

RNA was isolated from 5 dpf zebrafish larvae or adult zebrafish liver using an RNeasy kit (Qiagen, 74104), and cDNA was reverse transcribed using an EcoRry Premix (Takara-Clontech, 639543). Quantitative PCR (Kapa SYBR FAST qPCR kit, KK4602) was performed using a Rotor Gene Q qPCR machine (Qiagen). Primers used in RT-quantitative PCR were 5'-ggcttctgctctgtatgg-3' and 5'-ggctctgaccttggat-3' for zebrafish β -actin; 5'-ctcttctcactcctctgtt-3' and 5'-tggtcctctgtggtctctt-3' for zebrafish *ldlr*; 5'-ctaaccgacgccaagtga-3' and 5'-agacgacaacaacaacaac-3' for zebrafish *sreb1*; 5'-aggaggagtggtgaagga-3' and 5'-gttgatggaggagcgtag-3' for zebrafish *sreb2*; 5'-ctgctatctattgctgtg-3' and 5'-ttgaggaggaaggttagt-3' for zebrafish *hmgcr*; 5'-ctcgcctgaactgaactg-3' and 5'-tctaccgccgatagaa-3' for zebrafish *fasn*; and 5'-gaacaccactcaact-3' and 5'-cagctctctactact-3' for zebrafish *pcsk9*.

Oil Red O and BODIPY staining

For Oil Red O (ORO) staining, embryos or larvae were fixed in 4% paraformaldehyde for 2 h, washed three times in PBS, incubated in 0.3% ORO solution for 2 h, and then washed with PBS before imaging. For BODIPY staining, live larvae were immersed in E3 water (5.0 mM NaCl, 0.17 mM KCl, 0.33 mM CaCl₂, 0.33 mM MgSO₄) containing 0.1 μ g/ml BODIPY 505/515 (Invitrogen, D-3921) for 1 h in the dark and then rinsed with E3 water before imaging.

LPS treatment

Native *Escherichia coli* O111:B4 lipopolysaccharide (LPS) (Invitrogen, L4130), *Pseudomonas aeruginosa* LPS (Invitrogen, L9143),

and a fluorescent conjugate of LPS (Alexa Fluor 568-LPS/Alexa-LPS, Invitrogen, L23352) were dissolved in PBS to a stock concentration of 20 mg/ml. For intravenous LPS injection, 4.5 dpf embryos were laterally aligned in 0.5% low melting temperature agarose, and 5 nl of Alexa-LPS (1 mg/ml) were injected into the circulation through the cardinal vein using a Femtojet microinjector (Eppendorf). For the LPS survival challenge, 5 dpf larvae were immersed in water with different concentrations of *E. coli* LPS and *P. aeruginosa* LPS (100–1,000 µg/ml). Larvae survival, assessed by detectable heartbeat) was determined every hour after the immersion.

Imaging of live embryos or larvae

For in vivo microscopy, anesthetized embryos or larvae were mounted in 0.5% low melting temperature agarose (Sigma) containing tricaine (0.02%, Sigma) in 50 mm glass-bottom dishes (MatTek). Images were captured with a Leica CTR5000 or a BZ9000 Keyence fluorescent microscope. To quantify vascular lipid deposits, we captured a z-stack of 15 images in the trunk/tail region with a ×20 objective (BZ9000 Keyence). After overlaying images in the z-stack, using the BZ-X analyzer software (Keyence), vascular lipid deposits were manually counted in five consecutive vascular segments posterior to the anus.

RESULTS

Generation of an *ldlr* mutant with the CRISPR/Cas9 system

To create a loss-of-function *ldlr* mutant in zebrafish, we chose to use the CRISPR/Cas9 system (21). In zebrafish, there are two *ldlr* orthologs: *ldlra* (NCBI gene ID: 387529) and *ldlrb* (NCBI gene ID: 393460), with *ldlra* showing the higher degree of conservation with the human *LDLR* gene. The protein sequences between zebrafish *Ldlra* and human *LDLR* are conserved with an identity of 51.7% (supplemental Fig. S1), and the zebrafish *Ldlra* is predicted to have the conserved ligand-binding domain, epidermal growth factor precursor homology domain, and transmembrane domain. Hereinafter in this article, we designate *ldlra* as the *ldlr* gene in zebrafish. To disrupt *Ldlr* protein function with CRISPR/Cas9, we targeted the 5-prime of the *ldlr* coding region. Five *ldlr* genomic targets were chosen, and their corresponding gRNAs were synthesized. With T7 endonuclease digestion assay, we found one target, which is localized in exon 5, that was efficiently edited after Cas9/gRNA injection. The F0

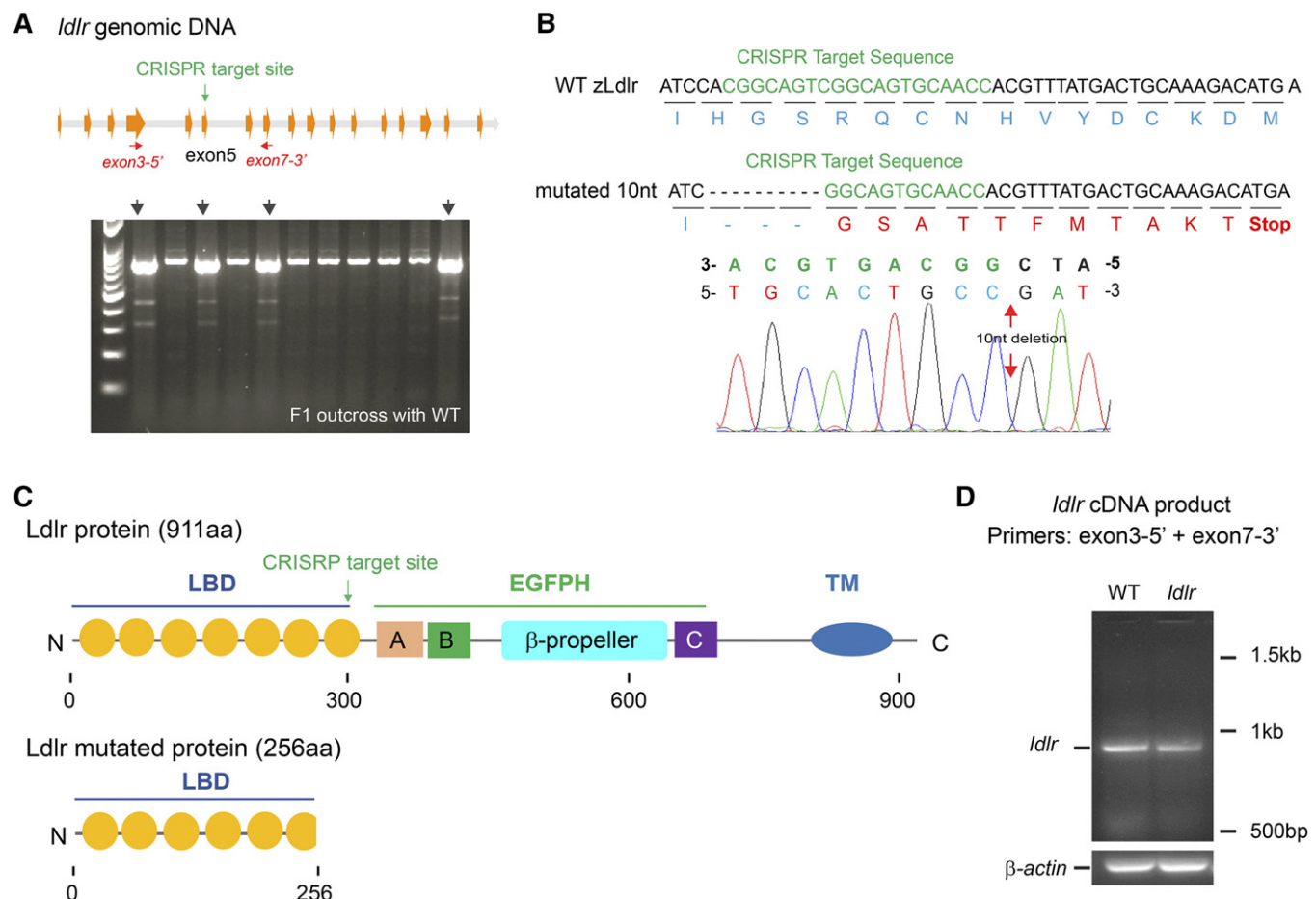


Fig. 1. Generation of an *ldlr* mutant with the CRISPR/Cas9 system. A: The genomic target site of CRISPR is located in exon 5. The heterozygotes from F1 outcross were identified by T7 endonuclease digestion. Black arrows point to heterozygotes. B: Sequences for a selected *ldlr* mutant, showing a 10nt deletion, which results in frame shift and prestop codon. C: Zebrafish *Ldlr* protein contains conserved ligand-binding domain, epidermal growth factor precursor homology domain, and transmembrane domain. The C-terminal domains required for *Ldlr* function are lost in the predicted truncated *Ldlr* mutant protein. D: cDNAs amplified from adult WT and *ldlr* mutant liver with primers flanking *ldlr* exon 3 and exon 7 have a single band of the similar size, indicating no alternative *ldlr* splicing transcripts in *ldlr* mutants. EGFP, epidermal growth factor precursor homology domain; LBD, ligand-binding domain; TM, transmembrane domain.

founder fish were raised and outcrossed with WT to obtain F1 generation. F1 were further outcrossed with WT to obtain F2 heterozygotes carrying the same mutation (Fig. 1A). In F1 generation, we screened the *ldlr* mutants and found one mutant line in which a fragment of 10nt was deleted, leading to a prestop codon (Fig. 1B). The truncated protein caused by the 10nt deletion and prestop codon in the *ldlr* mutant lost the whole C-terminal region, which is required for normal LDLR protein function (Fig. 1C). It is reported that frameshift indels may lead to in-frame exon skipping and alternative splicing (22). To check whether this 10nt deletion in exon 5 affected the splicing of the *ldlr* transcript, we designed primers for exon 3 and exon 7 to include exon 5 and the two neighboring exons. Semiquantitative PCR results from adult liver indicated decreased *ldlr* expression but no alternative splicing in the *ldlr* mutant (Fig. 1D), validating the predicted prestop codon. Therefore, this mutant line with the 10nt deletion was defined as our loss-of-function *ldlr* mutant and used in the following studies.

Hypercholesterolemia and activation of hepatic SREBP-2 pathway in adult *ldlr* mutants

It is well established that mutations in the LDLR C-terminal region that disrupt LDLR anchoring or processing

cause FH in human patients (4). To test whether truncated zebrafish Ldlr protein affects cholesterol homeostasis, we measured plasma lipid levels of the progenies from *ldlr* heterozygotes in-cross. Consistent with human and mouse studies, adult zebrafish homozygous *ldlr* mutants had significantly higher total cholesterol levels than did WT or *ldlr* heterozygote siblings when fed normal diet (Fig. 2A). Plasma triglyceride levels tended to be higher in homozygous *ldlr* mutants but were not significantly different from those in WT or heterozygotes (Fig. 2B). In agreement, neutral lipid staining of plasma separated on native gel suggested higher LDL, but lower VLDL in *ldlr* mutants, when compared with WT (Fig. 2C). Fast protein liquid chromatography data indicated that *ldlr* mutants had a much higher cholesterol levels in the IDL/LDL fractions. In contrast, *apoc2* mutants, reported in our earlier work (13) and used here as a control, showed higher cholesterol levels in the VLDL fraction (Fig. 2D). The TG levels were mildly increased in the LDL fraction in *ldlr* mutants but dramatically increased in the VLDL fraction in *apoc2* mutants, as was expected (Fig. 2E).

The LDLR is required for extracellular cholesterol uptake and regulation of the SREBP-2 pathway in the liver, the major organ responsible for plasma cholesterol regulation (3, 8). We next isolated liver from adult males and

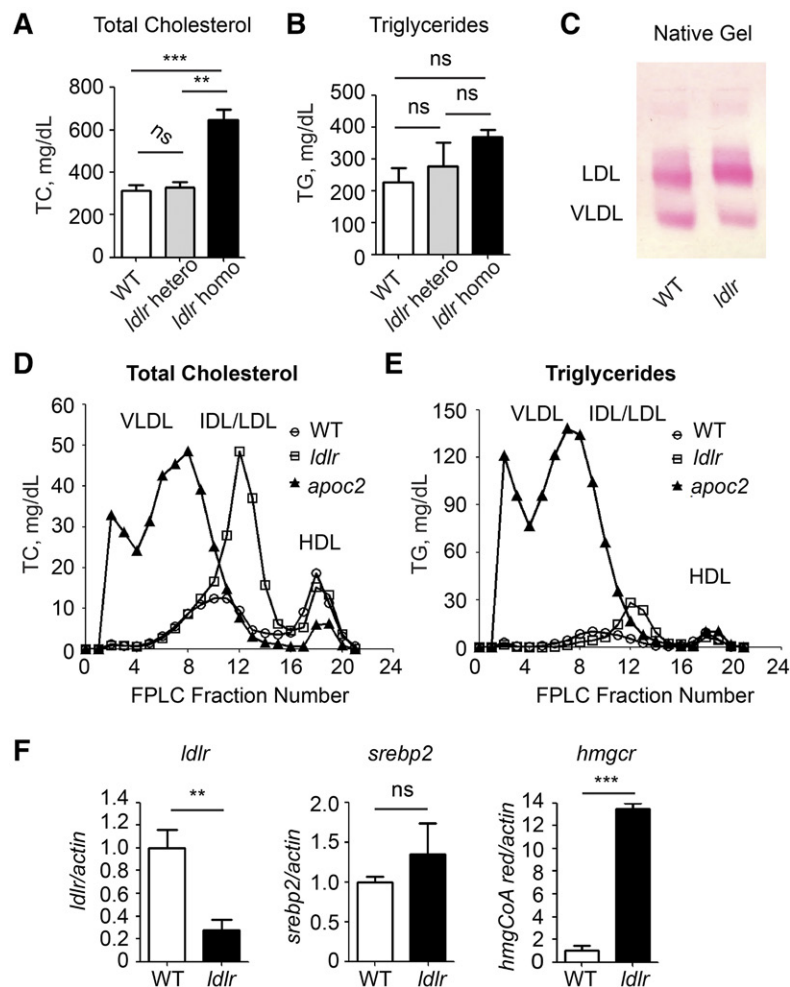


Fig. 2. Hypercholesterolemia and activation of hepatic SREBP-2 pathway in adult *ldlr* mutants fed normal diet. A, B: Plasma total cholesterol and triglycerides were measured in adult WT, *ldlr* mutant heterozygotes, and homozygotes, which were siblings in the same clutch, genotyped by T7 endonuclease digestion and sequencing ($n = 6$ for WT, $n = 4$ for *ldlr* hetero, and $n = 3$ for *ldlr* homo). C: Native electrophoresis and neutral lipid staining of plasma from adult WT and *ldlr* mutants. D, E: Fast protein liquid chromatography lipoprotein profile of pooled plasma from WT (30 animals), *ldlr* mutant (25 animals), and *apoc2* mutant (20 animals) zebrafish. F: Gene expression of *ldlr*, *srebp2*, and *hmgcr* in the liver of adult males ($n = 4$ in each group). FPLC, fast protein liquid chromatography. Mean \pm SEM; non-significant, $P > 0.05$; ** $P < 0.01$; *** $P < 0.001$ (Student's *t*-test).

extracted total RNA for qPCR. The *ldlr* mRNA levels were reduced by 75% in *ldlr* mutants, likely due to nonsense-mediated mRNA decay (23). Interestingly, although *srebp2* expression itself was not significantly changed, expression of *hmgcr*, the gene encoding HMG-CoA reductase and a major target gene of SREBP-2, was increased by as much as 13-fold (Fig. 2F).

Hyperlipidemia and activation of SREBP-2 pathway in *ldlr* mutant larvae

We next tested whether the *ldlr* mutant larvae had hyperlipidemia. Compared with WT, 5 dpf *ldlr* mutant larvae showed stronger vascular ORO and BODIPY staining (Fig. 3A, B), indicating elevated neutral lipid levels in the circulation. In agreement, total cholesterol and triglycerides

in larvae homogenates were significantly higher in *ldlr* mutants than in WT (Fig. 3C, D). To test SREBP-2 activation, we extracted total RNA for qPCR from 4 dpf WT and *ldlr* mutant larvae. There were no significant changes in *srebp1* or *srebp2* mRNA expression. However, there was a 4-fold increase in *hmgcr* expression and a 2-fold increase in fatty acid synthase (*fasn*) expression in *ldlr* mutants. Interestingly, expression of *pcsk9*, another SREBP-2 target, was not changed in *ldlr* mutants (Fig. 3E).

Increased vascular lipid accumulation in *ldlr* mutant larvae following short-term high-cholesterol feeding

We and others used zebrafish larvae to monitor vascular lipid accumulation in vivo (13, 14, 19, 20). In our previous studies, WT embryos were fed HCD for 2 weeks before

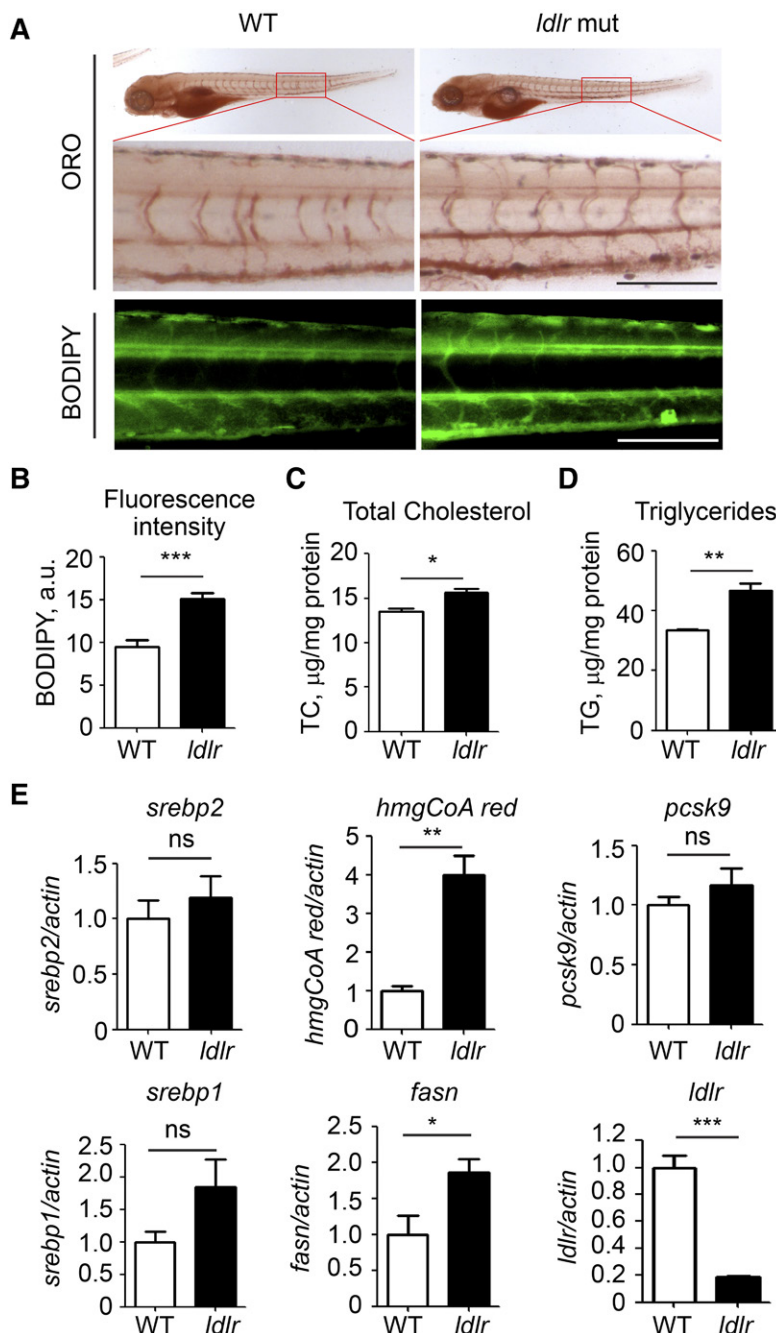


Fig. 3. Hyperlipidemia and activated SREBP-2 pathway in *ldlr* mutant larvae. A: ORO and BODIPY staining in 5 dpf WT and *ldlr* mutant larvae. Scale bars = 100 μ m. B: Quantification of BODIPY fluorescence intensity in 5 dpf WT and *ldlr* mutant larvae (n = 9 for WT and n = 11 for *ldlr* mutants). C, D: Total cholesterol and triglyceride levels in homogenates from 5 dpf WT and *ldlr* mutants (n = 4 in each group). E: Gene expression of *srebp1*, *srebp2*, *hmgcr*, *pcsk9*, *fasn*, and *ldlr* in the 4 dpf whole embryo (n = 4 in each group). Mut, mutant. Mean \pm SEM; ns, $P > 0.05$; * $P < 0.05$; ** $P < 0.01$; *** $P < 0.001$ (Student's *t*-test).

imaging vascular lipid deposits (14). Considering the hypercholesterolemia in nonfed *ldlr* mutant larvae, we tested whether an even shorter-term HCD feeding would induce vascular lipid accumulation. WT and *ldlr* mutants were fed control diet or HCD starting at 4.5 dpf. After a 5-day feeding, 9 dpf live larvae were immobilized in low-melting temperature agarose and imaged, as described (14, 20). When fed control diet, *ldlr* mutant larvae showed a moderate but significant increase in vascular lipid deposits in comparison with WT. When fed an HCD, *ldlr* mutant larvae displayed a dramatic increase in lipid deposits. In contrast, WT larvae did not accumulate vascular lipid deposits within this short time frame of HCD challenge (Fig. 4A, B). There were no apparent morphological or body-size changes in either WT or *ldlr* mutant larvae following HCD feeding (supplemental Fig. S2).

Our results indicate that the *ldlr* loss-of-function mutation has resulted in an increased susceptibility to a dietary cholesterol challenge, closely resembling the phenotypes observed in *Ldlr*^{-/-} mice (11, 12). To evaluate whether the new animal model in which *ldlr* mutant zebrafish are subjected to short-term (5 days) HCD feeding can be useful for drug screening, we tested effects of probucol, an antioxidant, and lomitapide, an MTP inhibitor, on vascular lipid accumulation. Both probucol and lomitapide have been shown to exert antioxidant and MTP inhibitor properties, respectively, in zebrafish (20, 24). As was expected, lomitapide decreased the plasma lipid levels in *ldlr* mutants, as assessed by ORO staining (Fig. 5A), by blocking their absorption in the intestine. Vascular lipid deposits were not decreased by probucol treatment but were significantly decreased by the treatment with lomitapide (Fig. 5B, C), suggesting that lipid levels, but not lipid oxidation, play a dominant role in early vascular lipid accumulation event in loss-of-function *ldlr* mutant larvae.

Decreased hepatic clearance of LPS in *ldlr* mutant larvae

LPS are found in the outer membrane of gram-negative bacteria and elicit strong immune response in animals, in extreme cases resulting in septic shock (25). Previous

studies have shown that hepatocytes are responsible for plasma LPS clearance, and this process is dependent on LDLR and its regulator, PCSK9 (26, 27). We tested these hypotheses using our new *ldlr* mutant zebrafish. At 4.5 dpf, WT and *ldlr* larvae were injected with red fluorescent Alexa-LPS. After 2 days, fluorescence signals were detected in both liver and vasculature (Fig. 6A). A ratio of Alexa-LPS fluorescence intensity in the liver to that in the vasculature was used as an index for hepatic LPS uptake. The *ldlr* mutant larvae had a decreased hepatic uptake of Alexa-LPS in comparison with WT (Fig. 6B). To test whether decreased hepatic clearance of LPS affects tolerance of zebrafish larvae to LPS challenge, we tested larvae survival following LPS exposure. Consistent with a previous report (28), we found that *P. aeruginosa* LPS induced more larval death than did the same doses of *E. coli* LPS (supplemental Fig. S3). The *ldlr* mutant larvae exposed to *P. aeruginosa* LPS had a lower survival than did WT (Fig. 6C). These results suggest that Ldlr-mediated hepatic clearance of LPS is important for zebrafish survival.

DISCUSSION

The goal of this work was to establish a genetic model of hypercholesterolemia in zebrafish. The *ldlr* mutant zebrafish developed in this study adds to the set of zebrafish models of lipid abnormalities and lipoprotein oxidation, which includes *apoc2* mutant zebrafish that develop severe hypertriglyceridemia (13), loss and gain of function liver X receptor mutants (29, 30), and *hsp70:IK17-EGFP* zebrafish that serve as a reporter for oxidation-specific epitopes (20), among others. We have previously been able to achieve hypercholesterolemia in WT zebrafish by feeding larvae an HCD for 2 weeks, which resulted in accumulation of vascular lipid deposits (14). This approach was further advanced by the introduction of a protocol in which an antisense morpholino oligonucleotide-mediated knockdown of *ldlr* allowed for shorter HCD feeding times to achieve meaningful hypercholesterolemia and vascular lipid accumulation (19). The introduction of our new *ldlr* mutant reduces the

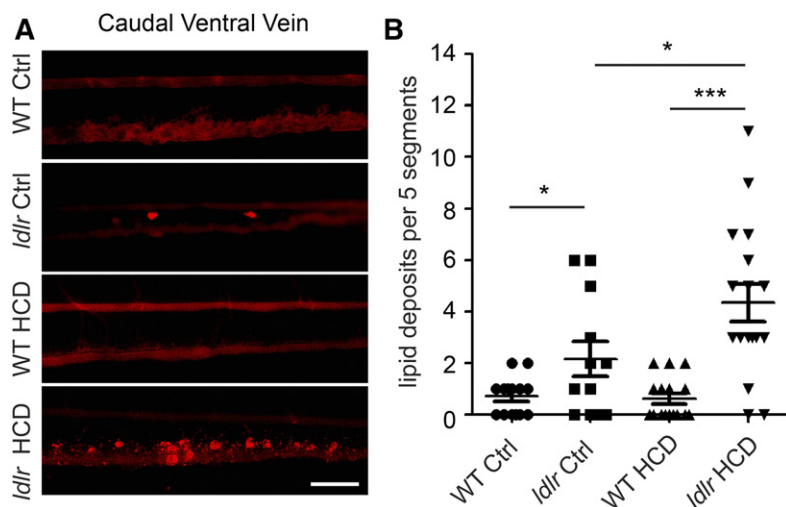


Fig. 4. Vascular lipid accumulation in *ldlr* mutants fed HCD. A: Representative images showing lipid deposits (bright red) in the caudal vein of 9 dpf WT and *ldlr* mutant larvae following 5-day feeding with control diet or HCD. Scale bar = 50 μ m. B: Quantitative results for a number of lipid deposits in a specified vascular area. Ctrl, control diet. Mean \pm SEM (n = 11–17 in each group). * P < 0.05; *** P < 0.001 (Student's *t*-test).

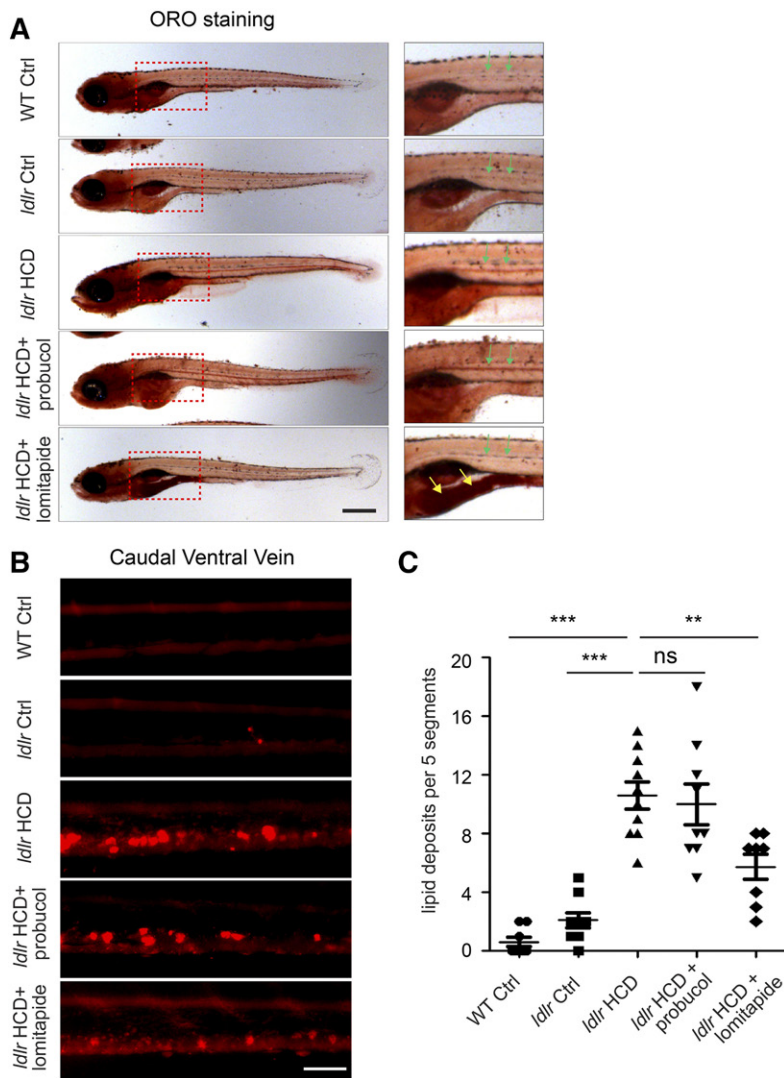


Fig. 5. Effects of probucol and lomitapide on hyperlipidemia and vascular lipid accumulation. **A:** ORO staining of 9 dpf larvae, following 5-day feeding with HCD, supplemented with probucol and lomitapide. Green arrows point to dorsal aorta, and yellow arrows point to intestine. Scale bar = 500 μm . **B, C:** Representative images and quantitative data for vascular lipid deposits. Scale bar = 50 μm . Mean \pm SEM ($n = 8-10$ in each group). ns, $P > 0.05$; ** $P < 0.01$; *** $P < 0.001$ (Student's t -test).

variability associated with morpholino oligonucleotide injections and feeding protocols and allows for achieving a robust and consistent phenotype.

The mutation we introduced into the zebrafish *ldlra* gene created a stop codon and resulted in a truncated, non-functional, and rapidly degraded *ldlr* transcript. The *ldlr*

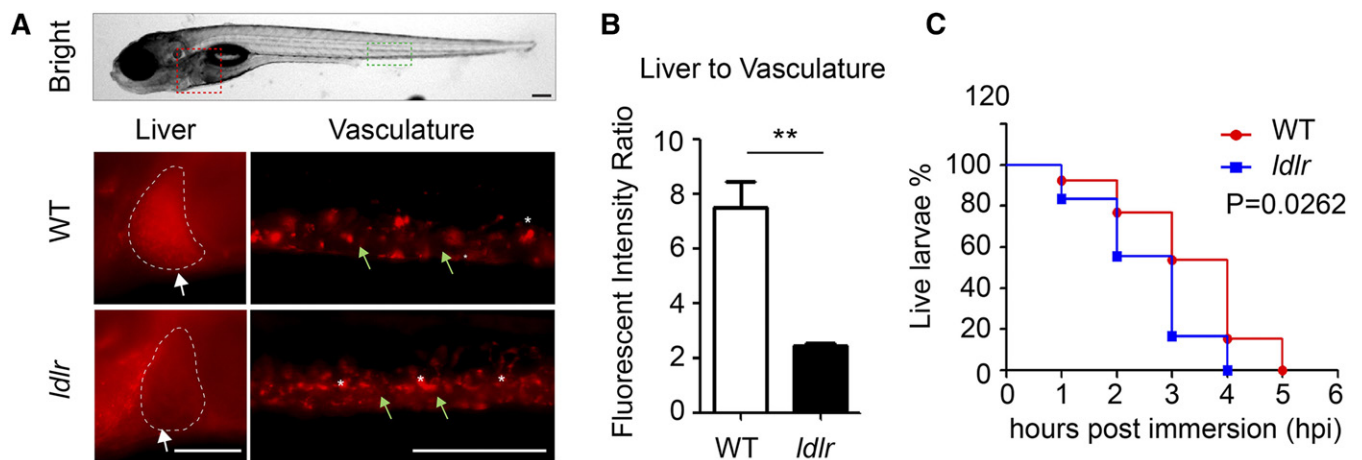



Fig. 6. Reduced hepatic uptake of LPS and survival of *ldlr* mutants upon LPS challenge. **A:** Representative images of 6.5 dpf WT and *ldlr* mutant larvae following Alexa-LPS injection (5 nl, 1 mg/ml) at 4.5 dpf. White and green arrows point to fluorescent signals in liver and the tail vasculature, respectively. Scale bars = 200 μm . **B:** Quantification of the ratio of fluorescent intensity in liver to that in vasculature. Mean \pm SEM ($n = 6$ for WT and $n = 5$ for *ldlr* mutant). ** $P < 0.01$ (Student's t -test). **C:** Survival curves for 5 dpf WT and *ldlr* mutant larvae following immersion in water with 500 $\mu\text{m}/\text{ml}$ *P. aeruginosa* LPS ($n = 13$ for WT and $n = 18$ for *ldlr* mutants). $P < 0.05$ (Log-rank Mantel-Cox test).

mutants fed a normal diet had moderate hypercholesterolemia and activated the SREBP-2 pathway, as is evident from the increased expression of *hmgcr*. Remarkably, as short as a 5-day HCD feeding resulted in robust vascular lipid accumulation in *ldlr* mutants. Lomitapide, but not probucol, prevented HCD-induced accumulation of vascular lipid deposits. We propose that a protocol using 5-day HCD feeding of *ldlr* mutant larvae can be used for mechanistic studies, as well as for initial genetic or drug screening to identify new therapeutic targets.

We also suggest that the advantage of using zebrafish is in the close similarity between zebrafish and human lipoprotein metabolism, as well as the differences that increase zebrafish propensity to developing hypercholesterolemia. Unlike mice, zebrafish express cholesteryl ester transfer protein, which helps retain cholesterol esters in the circulation. In addition, though mouse ApoB proteins are mostly ApoB48, which causes a rapid hepatic cycling of VLDL and low-atherogenic LDL levels (31), zebrafish do not express the apoB mRNA editing enzyme APOBEC1 (apolipoprotein B mRNA editing enzyme 1), and the majority of zebrafish ApoB protein is likely ApoB100, as our earlier studies suggest (32). ApoB100-containing LDL and VLDL remnants have a longer half-life time in plasma, adding to their atherogenicity. Indeed, the lipoprotein profile of normal diet-fed *ldlr* mutants shows a substantial IDL/LDL fraction, surpassing that seen in chow-fed *Ldlr*^{-/-} mice. This may explain, in part, why *ldlr* zebrafish larvae are so sensitive to HCD feeding and accumulate vascular lipid deposits within a short-time frame.

Interestingly, we found that HMG-CoA reductase was consistently and dramatically upregulated in *ldlr* mutant. However, other *srebp2* genes, including *pcsk9*, were not significantly changed. We propose that different target genes are regulated by SREBP-2 in a different manner, and it will be intriguing to explore the underlying mechanisms, which might provide new insights and suggest new approaches for differential targeting of genes regulating cholesterol homeostasis. Another interesting observation was the lack of the effect of probucol treatment on vascular lipid accumulation in 5-day HCD-fed *ldlr* mutants. This was in contrast to our previous results with 15-day HCD-fed WT zebrafish (20). This discrepancy may be explained, in part, by the different time scale of these experiments and disrupted hepatic uptake of LDL in *ldlr* mutants, which affects the LDL particle size and its vulnerability to oxidation.

In summary, this work introduces a new genetic model of hypercholesterolemia and early atherogenesis in which the *ldlr* zebrafish mutants subjected to a short, 5-day HCD feeding results in robust and consistent accumulation of vascular lipid deposits. We propose that this new animal model can be used for mechanistic studies and for the screening of new therapeutic targets and treatments. 

REFERENCES

1. Goldstein, J. L., and M. S. Brown. 2015. A century of cholesterol and coronaries: from plaques to genes to statins. *Cell*. **161**: 161–172.

2. Glass, C. K., and J. L. Witztum. 2001. Atherosclerosis. The road ahead. *Cell*. **104**: 503–516.

3. Goldstein, J. L., and M. S. Brown. 2009. The LDL receptor. *Arterioscler. Thromb. Vasc. Biol.* **29**: 431–438.

4. Hobbs, H. H., M. S. Brown, and J. L. Goldstein. 1992. Molecular genetics of the LDL receptor gene in familial hypercholesterolemia. *Hum. Mutat.* **1**: 445–466.

5. Brown, M. S., and J. L. Goldstein. 1986. A receptor-mediated pathway for cholesterol homeostasis. *Science*. **232**: 34–47.

6. Usifo, E., S. E. Leigh, R. A. Whittall, N. Lench, A. Taylor, C. Yeats, C. A. Orengo, A. C. Martin, J. Celli, and S. E. Humphries. 2012. Low-density lipoprotein receptor gene familial hypercholesterolemia variant database: update and pathological assessment. *Ann. Hum. Genet.* **76**: 387–401.

7. Cuchel, M., E. Bruckert, H. N. Ginsberg, F. J. Raal, R. D. Santos, R. A. Hegele, J. A. Kuivenhoven, B. G. Nordestgaard, O. S. Descamps, E. Steinhausen-Thiessen, et al., and European Atherosclerosis Society Consensus Panel on Familial Hypercholesterolaemia. 2014. Homozygous familial hypercholesterolaemia: new insights and guidance for clinicians to improve detection and clinical management. A position paper from the Consensus Panel on Familial Hypercholesterolaemia of the European Atherosclerosis Society. *Eur. Heart J.* **35**: 2146–2157.

8. Goldstein, J. L., R. A. DeBose-Boyd, and M. S. Brown. 2006. Protein sensors for membrane sterols. *Cell*. **124**: 35–46.

9. Rader, D. J., and J. J. Kastelein. 2014. Lomitapide and mipomersen: two first-in-class drugs for reducing low-density lipoprotein cholesterol in patients with homozygous familial hypercholesterolemia. *Circulation*. **129**: 1022–1032.

10. Gaudet, D., D. A. Gipe, R. Pordy, Z. Ahmad, M. Cuchel, P. K. Shah, K. Y. Chyu, W. J. Sasiela, K. C. Chan, D. Brisson, et al. 2017. ANGPTL3 inhibition in homozygous familial hypercholesterolemia. *N. Engl. J. Med.* **377**: 296–297.

11. Ishibashi, S., J. L. Goldstein, M. S. Brown, J. Herz, and D. K. Burns. 1994. Massive xanthomatosis and atherosclerosis in cholesterol-fed low density lipoprotein receptor-negative mice. *J. Clin. Invest.* **93**: 1885–1893.

12. Ishibashi, S., M. S. Brown, J. L. Goldstein, R. D. Gerard, R. E. Hammer, and J. Herz. 1993. Hypercholesterolemia in low density lipoprotein receptor knockout mice and its reversal by adenovirus-mediated gene delivery. *J. Clin. Invest.* **92**: 883–893.

13. Liu, C., K. P. Gates, L. Fang, M. J. Amar, D. A. Schneider, H. Geng, W. Huang, J. Kim, J. Pattison, J. Zhang, et al. 2015. Apoc2 loss-of-function zebrafish mutant as a genetic model of hyperlipidemia. *Dis. Model. Mech.* **8**: 989–998.

14. Stoletov, K., L. Fang, S. H. Choi, K. Hartvigsen, L. F. Hansen, C. Hall, J. Pattison, J. Juliano, E. R. Miller, F. Almazan, et al. 2009. Vascular lipid accumulation, lipoprotein oxidation, and macrophage lipid uptake in hypercholesterolemic zebrafish. *Circ. Res.* **104**: 952–960.

15. Gibbs-Bar, L., H. Tempelhof, R. Ben-Hamo, Y. Ely, A. Brandis, R. Hofi, G. Almog, T. Braun, E. Feldmesser, S. Efroni, et al. 2016. Autotaxin-lysophosphatidic acid axis acts downstream of apolipoprotein B lipoproteins in endothelial cells. *Arterioscler. Thromb. Vasc. Biol.* **36**: 2058–2067.

16. Fang, L., C. Liu, and Y. I. Miller. 2014. Zebrafish models of dyslipidemia: relevance to atherosclerosis and angiogenesis. *Transl. Res.* **163**: 99–108.

17. Anderson, J. L., J. D. Carten, and S. A. Farber. 2011. Zebrafish lipid metabolism: from mediating early patterning to the metabolism of dietary fat and cholesterol. *Methods Cell Biol.* **101**: 111–141.

18. Otis, J. P., E. M. Zeituni, J. H. Thierer, J. L. Anderson, A. C. Brown, E. D. Boehm, D. M. Cerchione, A. M. Ceasrine, I. Avraham-Davidi, H. Tempelhof, et al. 2015. Zebrafish as a model for apolipoprotein biology: comprehensive expression analysis and a role for ApoA-IV in regulating food intake. *Dis. Model. Mech.* **8**: 295–309.

19. O'Hare, E. A., X. Wang, M. E. Montasser, Y. P. Chang, B. D. Mitchell, and N. A. Zaghoul. 2014. Disruption of *ldlr* causes increased LDL-c and vascular lipid accumulation in a zebrafish model of hypercholesterolemia. *J. Lipid Res.* **55**: 2242–2253.

20. Fang, L., S. R. Green, J. S. Baek, S. H. Lee, F. Ellett, E. Deer, G. J. Lieschke, J. L. Witztum, S. Tsimikas, and Y. I. Miller. 2011. In vivo visualization and attenuation of oxidized lipid accumulation in hypercholesterolemic zebrafish. *J. Clin. Invest.* **121**: 4861–4869.

21. Jao, L. E., S. R. Wente, and W. Chen. 2013. Efficient multiplex biallelic zebrafish genome editing using a CRISPR nuclease system. *Proc. Natl. Acad. Sci. USA.* **110**: 13904–13909.

22. Lalonde, S., O. A. Stone, S. Lessard, A. Lavertu, J. Desjardins, M. Beaudoin, M. Rivas, D. Y. R. Stainier, and G. Lettre. 2017. Frameshift indels introduced by genome editing can lead to in-frame exon skipping. *PLoS One*. **12**: e0178700.
23. Wittkopp, N., E. Huntzinger, C. Weiler, J. Sauliere, S. Schmidt, M. Sonawane, and E. Izaurralde. 2009. Nonsense-mediated mRNA decay effectors are essential for zebrafish embryonic development and survival. *Mol. Cell. Biol.* **29**: 3517–3528.
24. Zeituni, E. M., M. H. Wilson, X. Zheng, P. A. Iglesias, M. A. Sepanski, M. A. Siddiqi, J. L. Anderson, Y. Zheng, and S. A. Farber. 2016. Endoplasmic reticulum lipid flux influences enterocyte nuclear morphology and lipid-dependent transcriptional responses. *J. Biol. Chem.* **291**: 23804–23816.
25. Molinaro, A., O. Holst, F. Di Lorenzo, M. Callaghan, A. Nurisso, G. D'Errico, A. Zamyatina, F. Peri, R. Berisio, R. Jerala, et al. 2015. Chemistry of lipid A: at the heart of innate immunity. *Chemistry*. **21**: 500–519.
26. Topchiy, E., M. Cirstea, H. J. Kong, J. H. Boyd, Y. Wang, J. A. Russell, and K. R. Walley. 2016. Lipopolysaccharide is cleared from the circulation by hepatocytes via the low density lipoprotein receptor. *PLoS One*. **11**: e0155030.
27. Walley, K. R., K. R. Thain, J. A. Russell, M. P. Reilly, N. J. Meyer, J. F. Ferguson, J. D. Christie, T. A. Nakada, C. D. Fjell, S. A. Thair, et al. 2014. PCSK9 is a critical regulator of the innate immune response and septic shock outcome. *Sci. Transl. Med.* **6**: 258ra143.
28. Dios, S., P. Balseiro, M. M. Costa, A. Romero, S. Boltana, N. Roher, S. Mackenzie, A. Figueras, and B. Novoa. 2014. The involvement of cholesterol in sepsis and tolerance to lipopolysaccharide highlighted by the transcriptome analysis of zebrafish (*Danio rerio*). *Zebrafish*. **11**: 421–433.
29. Cruz-Garcia, L., and A. Schlegel. 2014. Lxr-driven enterocyte lipid droplet formation delays transport of ingested lipids. *J. Lipid Res.* **55**: 1944–1958.
30. Benítez-Santana, T., S. E. Hugo, and A. Schlegel. 2017. Role of intestinal LXRalpha in regulating post-prandial lipid excursion and diet-induced hypercholesterolemia and hepatic lipid accumulation. *Front. Physiol.* **8**: 280.
31. Ishibashi, S., J. Herz, N. Maeda, J. L. Goldstein, and M. S. Brown. 1994. The two-receptor model of lipoprotein clearance: tests of the hypothesis in “knockout” mice lacking the low density lipoprotein receptor, apolipoprotein E, or both proteins. *Proc. Natl. Acad. Sci. USA*. **91**: 4431–4435.
32. Fang, L., R. Harkewicz, K. Hartvigsen, P. Wiesner, S. H. Choi, F. Almazan, J. Pattison, E. Deer, T. Sayaphupha, E. A. Dennis, et al. 2010. Oxidized cholesteryl esters and phospholipids in zebrafish larvae fed a high-cholesterol diet: macrophage binding and activation. *J. Biol. Chem.* **285**: 32343–32351.